IV International Conference on Particle-based Methods – Fundamentals and Applications
PARTICLES 2015
E. Oñate, M. Bischoff, D.R.J. Owen, P. Wriggers & T. Zohdi (Eds)

OPTIMAL PARTICLE PARAMETERS FOR CLC AND CLR PROCESSES - PREDICTIONS BY INTRA-PARTICLE TRANSPORT MODELS AND EXPERIMENTAL VALIDATION

THOMAS FORGBER,[1] JULIAN R. TOLCHARD,[2] ABDELGHAFOUR ZAABOUT,[2] PAUL INGE DAHL,[2] AND STEFAN RADL[1]

[1] Institute of Process and Particle Engineering
Graz University of Technology, Graz, Austria
e-mail: radl@tugraz.at, thomas.forgber@tugraz.at, URL: http://ippt.tugraz.at

[2] SINTEF Materials and Chemistry
e-mail: Julian.R.Tolchard@sintef.no, Abdelghafour.Zaabout@sintef.no, PaulInge.Dahl@sintef.no
URL: http://www.sintef.com/home/SINTEF-Materials-and-Chemistry

Key words: Granular Materials, Heterogeneous Reactions, Chemical Looping Combustion, Chemical Looping Reforming.

Summary. *Validated models for predicting oxidation and reduction kinetics of multi-component porous particles in chemical looping combustion (CLC) and chemical looping reforming (CLR) processes are of key importance to identify the rate limiting step in these processes. Since particle properties (i.e., their composition, porosity, pore size, grain size, etc.) can be adjusted by modern synthesis techniques, there is an open question on the optimal set of these properties that would lead to the most economic process. We introduce a general open-source simulation environment, called ParScale that can be used to simulate models relevant for CLC and CLR processes, and hence can be used for their optimization. Most important, ParScale features a generalized one-dimensional spherical discretization which enables the user to predict an arbitrary number of reactions within non-isothermal porous particles consisting of multiple solid (reactive or inert) species. We perform an optimization study (constrained by typical process requirements like the maximum reaction time) for an isothermal first-order reaction, as well as for an n-th order reaction typical for hematite reduction. Finally, materials consisting of active nanoparticles embedded in a matrix of a different composition are synthesized and analyzed.*

1 INTRODUCTION

The modeling of heterogeneous reactions occurring at the inner surface of porous particles is an important tool for the design of CLC and CLR processes. These processes typically consist of two reactors, the first being a so-called air reactor in which a metal (or metal oxide, e.g., FeO, denoted here as the "carrier") is oxidized. In a second reactor, the metal oxide is used to oxidize a fuel (e.g., methane, in case of CLC), or partially oxidize a fuel to produce hydrogen or syngas (in case of CLR) [1,2]. Despite the potential economic advantages and the great scientific interest in these processes, it is still unclear which particle configuration leads to a cost-optimal operation. Modeling of CLC and CLR processes can help to identify such

optimal conditions, and minimize costly and tedious experiments.

Particle-scale models for CLC and CLR describe intra-particle reaction-advection-diffusion phenomena, as summarized in the recent work of Noorman et al. [3]. Key phenomena that need to be modeled include (i) Maxwell-Stefan multi-component gas diffusion, (ii) gas-phase convective transport, and (iii) the heat release due to one or multiple heterogeneous reactions. While analytical solutions exist in some limiting cases [4], a non-uniform initial active solids distribution within the particle, time-depended boundary conditions, or the coupling to external flow models (e.g., CFD) require the adoption of a numerical solution strategy [5,6]. Unfortunately, there exists no open-source particle-scale modeling toolbox that performs such a numerical integration, and which can be easily coupled to existing DEM or CFD-DEM simulators. Also, grain models [7] that model changes of the inner pore structure of the particle due to non-catalytic reactions, e.g., the formation of a product layer, are typically note considered [3].

1.1 Goals and Outline

This contribution focusses on the above issues by first introducing the open-source simulation tool *ParScale* [8]. *ParScale* is designed as a library to be linked to existing Lagrangian-based particle flow simulators, and is already integrated with the DEM-based simulator *LIGGGHTS*®.

First, we will introduce a rigorous grain-scale model that accounts for the effect of a porous matrix layer on the grains, and the formation of a dense product layer that slows down non-catalytic heterogeneous reactions. Second, we present results of an optimization study that is based on an analytical solution for a first-order reduction of hematite, as well as on *ParScale* simulations for a more general *n*-th order reaction. Specifically, we ask the question: "What is the optimal hematite loading of an otherwise inert support particle, and how does the porosity and pore size of the support particle influence this optimum?". Clearly, such an optimum must exist, since for a given pore size (of the support particle), a higher active solids loading (i.e., an increase in the solids volume fraction ε_s) leads to a smaller pore diameter d_s:

$$\frac{d_s}{d_{pore}} = \sqrt{1 - \frac{\varepsilon_s}{\phi_G \, \varepsilon_{support}}} \tag{1}$$

Here $\varepsilon_{support}$, d_{pore}, and ϕ_G is the porosity and the pore size of the support material, as well as the solids content of the grain layer, respectively (see Figure 1). In our model we assume that the grains of constant size and covered with a porous matrix layer with diameter d_M, are deposited at the walls of cylindrical pores. Thus, when increasing the active solids content, the available surface area of the grains, and hence the total reaction rate, increases. However, diffusion in the pores becomes slower due to (i) the lower overall porosity of the particle, and (ii) Knudsen effects (i.e., the overall diffusion coefficient D_{tot} and the diffusion parameter Ψ decrease with decreasing d_s, since the Knudsen diffusivity D_{Kn} decreases linearly with d_s):

$$D_{Kn} = \frac{d_s}{3} \sqrt{\frac{8 R_g T}{\pi MW_i}} \tag{2}$$

$$D_{tot}^{-1} = D_{mol}^{-1} + D_{Kn}^{-1} \tag{3}$$

$$\Psi = D_{tot} / D_{mol} \tag{4}$$

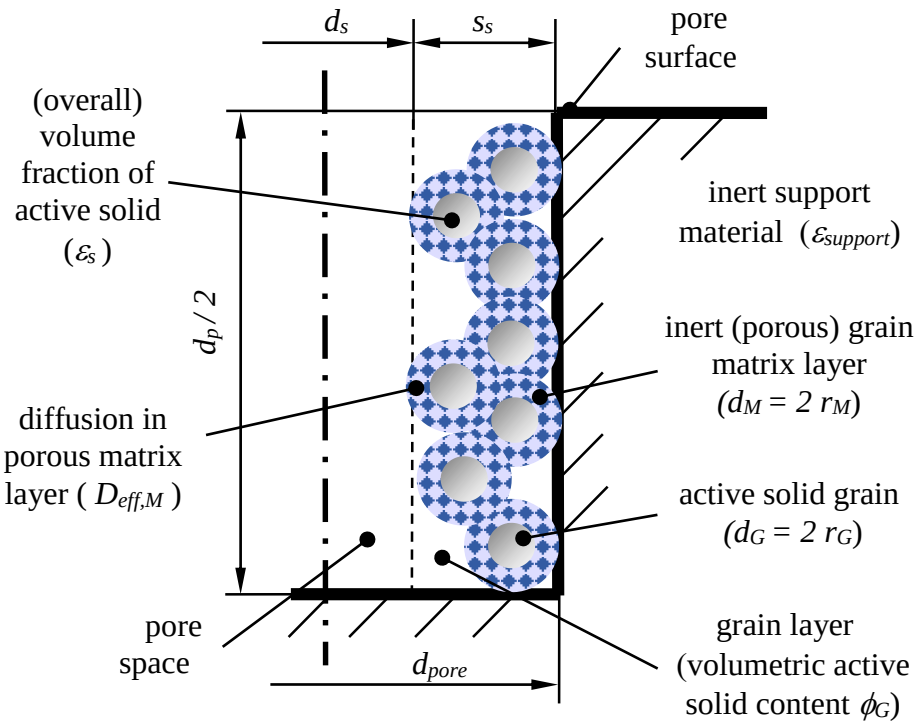

Figure 1. Model of a single pore including grain layer model.

2 POROUS PARTICLE MODEL

In order to introduce key dimensionless quantities, we now consider mole-based species transport equations and account for accumulation, diffusion and reaction of species i in a spherical porous particle. The (mole-based) volumetric source term in these transport equations due to a single chemical reaction, and in case only one gas-phase species and the active solid influence the reaction rate, is modelled as:

$$s_i = \nu_i\, k\, c_s^m\, c_i^n \tag{5}$$

Here ν_i is the stoichiometric constant of gas-phase species i, c is the concentration, and k is a volume-based reaction rate parameter (see next Chapter for details). m and n indicate the order of the reaction with respect to the active solid and gas-phase species, respectively. The resulting dimensionless transport equations for gas species i and the active solid (in which dimensionless quantities are indicated by an asterisk) are:

$$\partial_{t^*}\left(\varepsilon\, c_i^*\right) = \frac{1}{\xi^2}\partial_\xi\left(\xi^2\, \partial_\xi c_i^*\right) + \nu_i^* \Phi^2 c_i^{*n}, \tag{6}$$

$$\partial_{t^*}\left(c_s^*\right) = \nu_s^* \Phi^2 c_i^{*n}\, \frac{c_{i,0}}{c_{s,0}}\, \frac{|\nu_s|}{|\nu_i|}. \tag{7}$$

Here the reference quantities for the length, the time and the concentration are the particle radius $d_p/2$, the diffusion time $t_{diff} = d_p^2/4/D_{eff}$, and the reference (i.e., bulk) concentration $c_{i,0}$ of the gas-phase reactant, respectively. D_{eff} is the effective diffusion coefficient taking the particle porosity ε and tortuosity τ into account:

$$D_{eff} = D_{tot}\,\varepsilon / \tau\,. \tag{8}$$

The key dimensionless reaction parameter is the Thiele modulus

$$\Phi^2 = \frac{d_p^2 \left|\nu_i\right| k\, c_s^m\, c_{i,0}^{n_i - 1}}{4 D_{eff}}, \tag{9}$$

and the dimensionless boundary condition for the above partial differential equation is

$$\partial_{\xi} c_i^* = Bi\left(1 - c_i^*\right) / 2, \tag{10}$$

where $Bi = Sh\, D_{mol} / D_{eff,i}$. Note that the above equations neglect multi-component diffusion effects, and the drift flux, since these effects are often small [3]. More details regarding individual models and the approximations made are detailed in the *ParScale* online documentation [8].

3 GRAIN MODEL

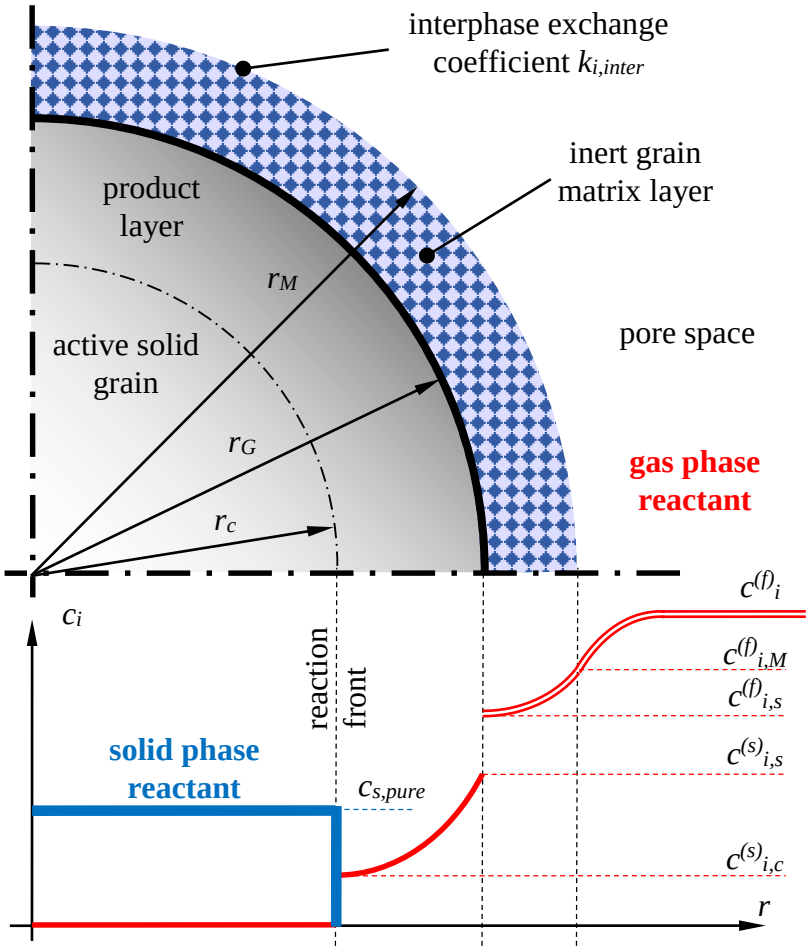

Figure 2. Grain-scale model including concentration profiles of the solid and the gas-phase reactant ($c_{s,pure}$ is the molar concentration of pure solid, which is different from the particle-average solid concentration $c_{s,0}$).

For a general heterogeneous reaction, the reaction rate parameter k in the above particle model is affected by (i) a surface area-specific reaction parameter k_s, (ii) the volume-specific

surface area of the active solid, and (iii) grain-scale effects (e.g., the formation of a product layer on, or in the spherical grains). In what follows, we show how k and k_s are related for a single non-catalytic reaction that is first-order (i.e., n = 1) with respect to the gas phase reactant. Specifically, we assume that the rate of reaction is affected by diffusion through an inert porous grain matrix layer, by dissociation/dissolution in a non-porous product layer (e.g., an active metal), as well as diffusion of the dissolved gas-phase reactant through the product layer to the reaction front (see Figure 2). All this is done in the context of a shrinking core type of model, assuming spherical monodisperse grains. Such a type of model and approach is typically adopted for grain-scale models, since it allows the derivation of an analytical expression for the volumetric reaction rate k [7]. Also, our idea of using a shrinking core type of model is justified by the formation of a rather sharp reaction front that forms between the educt and product layer in typical applications, i.e., in the $Fe_2O_3/Fe_3O_4/FeO$ system [9]. Due to the lack of more detailed diffusion and phase equilibrium data, we (i) model the phase equilibrium at the active solid grain / matrix layer interface using the constant H_i, and (ii) assume that the rate of diffusion is proportional to the gradient of the concentration of dissolved gas-phase reactant. Future work may incorporate more realistic approaches for modeling diffusion and phase equilibria in the active solid and the product layer (see, e.g., Ågren [9], or Kattner and Campbell [10]). Under the above assumptions, the gas consumption rate of a single grain $\dot{N}_i$ (in [kmol/s]) is governed by transport (R_{inter}, R_M, R_G) and reaction resistances (R_{react}) in the grain:

$$\dot{N}_i = 4\pi c_i^{(f)} / \left[R_{inter} + R_M + H_i \left(R_G + R_{react} \right) \right], \tag{11}$$

$$R_{inter} = 1/\left(r_M^2 k_{i,inter} \right), \tag{12}$$

$$R_M = \frac{1}{D_{eff,M}} \left(\frac{1}{r_G} - \frac{1}{r_M} \right), \tag{13}$$

$$R_G = \frac{1}{D_G} \left(\frac{1}{r_c} - \frac{1}{r_G} \right), \text{ and} \tag{14}$$

$$R_{react} = 1/\left(\nu_i \, k_s \, c_{s,pure} \, r_c^2 \right). \tag{15}$$

Here $c^{(f)}_i$ is the concentration of the gas-phase reactant in the pore space and at the grain position. Since we use a one-dimensional discretization of the porous particles, $c^{(f)}_i$ is only a function of the radial distance in the porous support, and is obtained by solving the transport equations presented in the last chapter. We now introduce a dimensionless radial position of the reaction front ξ_c in the grain, as well as a fractional conversion X_G of the grain:

$$\xi_c = r_c / r_G \tag{16}$$

$$X_G = 1 - \xi_c^3 \tag{17}$$

The latter, i.e., X_G, can be calculated from the particle-scale transport equations, and hence can be used to close the grain-scale model equations. Finally, we define a correction factor f that only depends on the conversion X_G of the grain and a set of constant parameters:

$$\dot{N}_i = \nu_i \, 4\pi r_G^2 \, f \, k_s \, c_{s,pure} \, c_i^{(f)} \tag{18}$$

$$f^{-1} = f_{inter+M}^{-1} + f_G^{-1} + f_{react}^{-1} \tag{19}$$

$$f_{inter+M}^{-1} = \nu_i \, r_G^2 \, k_s \, c_{s,pure} \left(\frac{1}{r_M^2 k_{i,inter}} + \frac{1}{D_{eff,M}} \left(\frac{1}{r_G} - \frac{1}{r_M} \right) \right) \tag{20}$$

$$f_G^{-1} = H_i \, \nu_i \, r_G \, k_s \, c_{s,pure} \left[\left(1 - X_c\right)^{-1/3} - 1 \right] / D_G \tag{21}$$

$$f_{react}^{-1} = H_i \left(1 - X_c\right)^{-2/3} \tag{22}$$

Note, that these expressions reduce to the result presented by Melchiori and Canu [7] in (i) the absence of a matrix layer, (ii) infinitely fast interphase mass transfer (i.e., $k_{i,inter} = \infty$), and (iii) in case we set $H_i = 1$ (since Melchiori and Canu [7] did not model dissolution and diffusion of gas-phase reactants in a solid, there was no need to describe a phase equilibrium in this previous work). Also, we have set $m = 0$ and have used the (constant) concentration $c_{s,pure}$ of the pure solid to compute the reaction rate. By doing so, the grain model will account for the change of the reaction rate due to the conversion of the solid. We can now relate the grain-based and the volume-based reaction rate parameter:

$$k = \left(6 / d_G\right) \varepsilon_s \, f \, k_s \, c_{s,pure} \tag{23}$$

Note, that for the general case of an n-th order reaction, no analytical solution for the correction factor f exists. Also, the dependency of f on the solids conversion leads to a non-linear particle model even in case $n = 1$. Hence, it is natural to consider a hypothetical situation in which $n = 1$, and no grain effects exist (i.e., $f = 1$). We adapt such a view in the next chapter to demonstrate our optimization strategy.

4 OPTIMAL PARAMETERS FOR FIRST-ORDER REACTIONS

4.1 Optimization strategy

In case we consider a reaction with $m = 0$, $n = 1$, and $f = 1$, analytical expressions for the temporal evolution of the concentration profiles $c_i(r)$, and $c_s(r)$ can be derived [4]. We hence have adopted such a parameter set, which has been also used to verify the correct implementation of the governing equations in *ParScale*. Specifically, we have used the oxidation of copper as presented by Noorman et al. [3] as the verification case. The setup and the results of this verification study which can be accessed online.

Furthermore, it is useful to define an instantaneous particle-averaged reaction rate $\overline{s} = \eta \, k \, c_{i,0}$, which depends on the concentration profiles (see, e.g., [4]). Here η is a (dimensionless) effectiveness factor that is a function of Φ and Bi. While the effect of Bi is typically weak, Φ (and hence η) is affected by the porosity ε and the pore diameter d_s. Both ε and d_s decrease with increasing solids loading ε_s as illustrated in Figure 1. η is time-invariant for the first stage of the reaction in which the solid-phase reactant is available over the full radial distance of the particle (clearly, the solid-phase reactant will deplete first at $r = d_p/2$, leading to an unreactive outer shell of the particle, ending the first stage of the reaction). It is now easy to observe that

$$\overline{s} \propto \eta \, \varepsilon_s \, k_s \, c_{s,pure} \, c_{i,0} / d_G \,. \tag{24}$$

Hence, one can maximize the particle-averaged reaction rate by (i) maximizing the surface-area specific reaction rate k_s, (ii) maximizing the gas-phase concentration, (iii)

minimizing the grain diameter, and by (iv) maximizing the product of the effectiveness factor and the solids loading ε_s. In case we would like to take grain-scale effects into account, we must maximize f as well. Clearly, f is at a maximum in case of (i) a thin matrix layer (i.e., r_M is close to r_G), (ii) large diffusivities in the grain matrix and in the product layer, (iii) a large gas solubility in the product layer (i.e., low H_i), and (iv) a large interphase exchange coefficient $k_{i,inter}$. Since it is clear which factors lead to an optimal f, and to keep the analysis simple by avoiding the introduction of unknown parameters, grain-scale effects are not considered in what follows.

4.2 Base case parameters

We now aim on maximizing $\eta\,\varepsilon_s$ for a typical CLC/CLR by varying the solids loading. The system under consideration is characterized by the base case parameters shown in Table 1.

Table 1. Base case parameters used for the optimization.

Parameter	Value	Parameter	Value
$\varepsilon_{support}$	0.5	ν_i	-4
τ	1.5	T	1098 [K]
d_p	100 [µm]	p	1 [bar]
d_{pore}	200 [nm]	Sh	2
ϕ_G	0.5	*gas properties*	CH_4 in N_2

4.3 Results

In Figure 3 (left panel) we plot the optimal solids loading normalized with the maximum possible solids loading (i.e., in case the pores are completely filled with solid reactant). A normalized reaction rate is shown on the horizontal axis in Figure 3. Therefore, we have defined a reference Thiele modulus Φ_{ref} based on a hypothetical maximum reaction rate k_{max} (that would be observed at the maximal possible solids loading), and the effective diffusion coefficient in the porous support at zero solids loading:

$$\Phi_{ref}^2 = d_p^2 \left|\nu_i\right| k_{\max} / \left(4 D_{eff,support}\right). \tag{25}$$

Our results summarized in Figure 3 indicate that

- the optimal solids loading is close to the maximum solids loading for slowly reacting systems (i.e., small Φ_{ref}). For highly reactive systems, however, the maximum solids loading should be in the range of 40 to 50% of the maximum possible solids loading. This is due to the fact that the decrease of the effective diffusion coefficient upon an increase in the solid loading outweighs the gain in the reactivity already at low ε_s.
- the pore size of the support has only a small effect on the optimal relative active solid loading. The only limitation is hence that pores must be large enough to deposit the active solid inside the pores. Also, pores should be small enough to keep the layer of deposited grains as thin as possible.
- as expected, the importance of Knudsen diffusion (quantified by the parameter Ψ_{opt}) increases for smaller pore diameters. Clearly, Knudsen effects need to be considered for all pore sizes considered, since Ψ_{opt} is substantially smaller than unity.

- there is no effect of the porosity of the support on the optimal relative metal loading at constant pore size (data not shown). Thus, in order to maximize the solids loading, the porosity of the support matrix should be as high as possible.

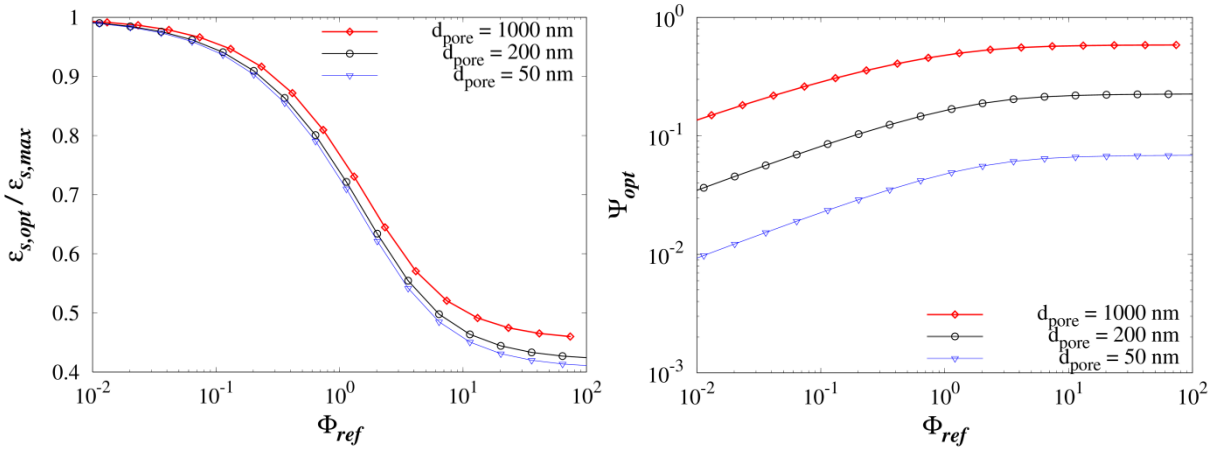

Figure 3. Optimal relative metal loading (left panel) and optimal dimensionless diffusivity (right panel) for various pore sizes.

5 OPTIMAL METAL OXIDE LOADING FOR THE REDUCTION OF HEMATITE

5.1 Reaction mechanism

We now consider the reduction of hematite (Fe_2O_3) using methane. Previous work on the Fe_2O_3/CH_4 system has been done by Monazan et al. [11], which proposed a reaction scheme consisting of two parallel reactions. Previous work did not take inter-particle transport limitations into account, since a fine-grained powder was used in the experiments, and the effect of support on the reaction outcome was not modeled. No detailed analysis regarding the catalytic effect of the metal was considered in previous work. Hence, we consider these previous results as the grain-scale reaction rates, which already account for the product layer formation. Consequently, we have not employed the grain model in what follows.

Following Monazan et al. [11], we adopt the following reactions (note, that hematite was modified with traces of Mg in previous work to accelerate the reaction)

$$4\mathrm{CH_4} + 27\mathrm{Fe_2O_3} \rightarrow 18\mathrm{Fe_3O_4} + 2\mathrm{CO_2} + 2\mathrm{CO} + 3\mathrm{H_2O} + 5\mathrm{H_2} \quad \text{(R.1)}$$

$$3\mathrm{CH_4} + 8\mathrm{Fe_3O_4} \rightarrow 24\mathrm{FeO} + 2\mathrm{CO_2} + \mathrm{CO} + 3\mathrm{H_2O} + 3\mathrm{H_2} \quad \text{(R.2)}$$

A typical conversion rate expression for these reactions is (only valid at zero conversion; for higher conversions the rate decreases appreciably):

$$\partial_t X_i = w_i \, X_\infty \, y_{\mathrm{CH_4}}^{n_i} \, k_i \exp\left[-E_{A,i} / T\right] \quad (26)$$

with the closures

$$w_1 = 1 - w_2 \quad (27)$$

$$w_2 = -0.828 + 0.0017\,\mathrm{T} + 0.1404\, y_{\mathrm{CH_4}} \quad (28)$$

$$X_\infty = 1.366 - 4.180 \cdot 10^5 / T^2 + 18.05 y_{\mathrm{CH_4}}^3 \quad (29)$$

$$k_1 = 383.9; k_2 = 144.6; n_1 = 0.182; n_2 = 0.272 \quad (30)$$

$$E_{A,1} = 6040; E_{A,2} = 7798 \tag{31}$$

The conversion rate is connected to the molar reaction rate s_i via:

$$s_{\mathrm{Fe_2O_3},i} = \partial_t X_i \frac{(1-\varepsilon)\rho_{\mathrm{Fe_2O_3}}}{MW_{\mathrm{Fe_2O_3}}} \tag{32}$$

The results of Monazan et al. [11] indicate conversion rates (typical for 825°C and y_{CH4} = 0.10) between 0.04 (for reaction R2) and 0.4 [min^{-1}] (for reaction R1). Thus, a typical reaction time scale is 2.5 and 25 minutes of the first and second reaction, respectively (i.e., R2 is substantially slower than R1). Assuming a particle porosity of ε = 0.5, pure Fe_2O_3 particles, a density of pure Fe_2O_3 of 5,240 [kg/m³], as well as a molecular weight of 160 [kg/kmol] (see Han et al., [5]), this translates into a typical iron oxide consumption rate s_{Fe2O3} of ca. 0.11 [kmol/m³/s], and a corresponding reaction rate of $R_{R1} = 4.1 \cdot 10^{-3}$ [kmol/m³/s]. When neglecting the effect of y_{CH4} on X_∞, and the effect of w_1 in the conversion rate expression, the following expression for the (linearized) reaction rate (exactly valid only for y_{CH4} = 0.10 and at 825°C) can be extracted from literature:

$$r_i = 6.23 \cdot 10^{-3} y_{\mathrm{CH_4}}^{0.182} \left[\frac{kmol}{m_{tot}^3 s} \right] \tag{33}$$

5.2 Concentration profiles

We consider the reduction of a hematite-impregnated porous support at different hematite loading levels ε_s (parameters are as shown in Table 1, with the exception of: d_p = 1 [mm], Bi = ∞, and y_{CH4} = 0.20; the characteristic reaction time scale in the absence of pore diffusion effects was set to 60 [s] in order to model reaction R1). Since the reaction order is n < 1, *ParScale* was used to solve the governing equations for the gas- and solid-phase concentration profiles. Figure 4 highlights the effect of the relative solids loading level ε_s on these profiles. ε_s affects both (i) the volumetric reaction rate, as well as (ii) the effective rate of diffusion in the pores, and consequently Φ.

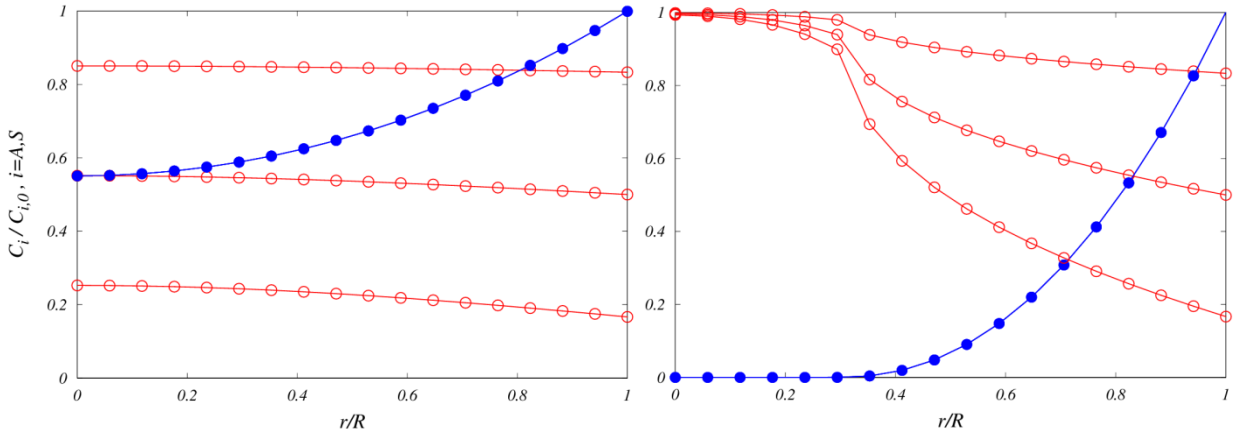

Figure 4. Normalized concentration profiles of gas (blue dots) and Fe_2O_3 (red circles, t = 10, 30, 50 [s] from top to bottom; left panel: ε_s / $\varepsilon_{s,max}$ = 0.90, Φ = 1.70; right panel: ε_s / $\varepsilon_{s,max}$ = 0.96, Φ = 3.39).

Interestingly, for high hematite loadings (see right panel in Figure 4) a rather sharp front in the hematite concentration profile develops at $r/R \sim 0.3$. Also, the results for the smaller Thiele modulus (see left panel in Figure 4) indicate a uniform solids concentration profile. In contrast, the concentration profile of the gas-phase reactant has a significant gradient. This is due to the insensitivity of the reaction rate on the methane concentration indicated by the small value of n.

5.3 Optimal solids loading

The variation in the solids loading both effects the particle-averaged reaction rate $\bar{s}$, as well as the final solids conversion after a pre-defined amount of time. We have decided to consider the latter in the following optimization analysis, since it is closer to the final application. Specifically, we have considered that the particles have a residence time of t_{res} = 100 [s] in the reduction reactor. The function to optimize is hence the total amount of consumed active solid per m³ of particle:

$$c_{s,t_{res}} = c_{s,0}\, X_s\left(t_{res}\right) \tag{34}$$

Note, that the initial (particle-averaged) solids concentration is related to ε_s:

$$c_{s,0} = \varepsilon_s \rho_s / MW_s \tag{35}$$

The results of the optimization study are summarized in Figure 5. Our data indicates that for the comparably slow reaction of CH_4 with hematite, the optimal solids loading is in the range of 85% to 95% of the maximal possible loading, depending on the pores size. This is in line with the findings summarized in Chapter 4 for a first-order reaction.

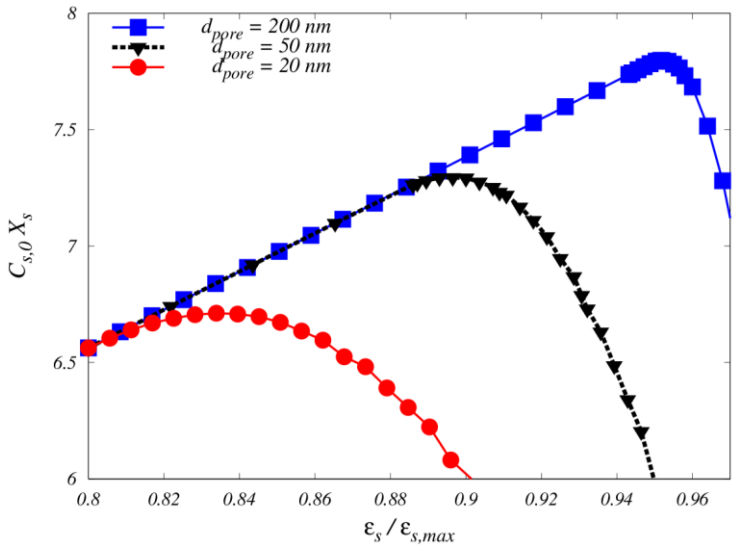

Figure 5. Normalized metal consumption as a function of the relative metal loading and pore size of the support.

6 EXPERIMENTAL VALIDATION

To work towards a validation of the presented models, as well as to investigate the thermochemical compatibility, commercially available Fe_2O_3 nanoparticles were embedded in a highly porous support matrix of $SrAl_6O_{19}$. The support matrix was synthesized through a

sol-gel route adapted from the method reported by Solunke et al. [12]. The active Fe_2O_3 nanoparticles and the highly porous support material are depicted in Figure 6. The Fe_2O_3 nanoparticles are not spherical as in the grain model, but are rather rod shaped with a width of 10-15 nm and a length in the range of 50-100 nm. Future work will attempt to quantify the effect of the grain shape on the conversion. Also, smaller and more spherical nanoparticles may be synthesized in future work, enabling us to fill even small pores in the support matrix. The BET specific surface area of the synthesized matrix material (with nanoparticles embedded) was measured to be 363 m^2/g, with a typical pore diameter in the lower mesoporous range (~5 nm). The matrix material is expected to coarsen, and the pores will widen during cycling at relevant operating temperatures (i.e., 600-900 °C).

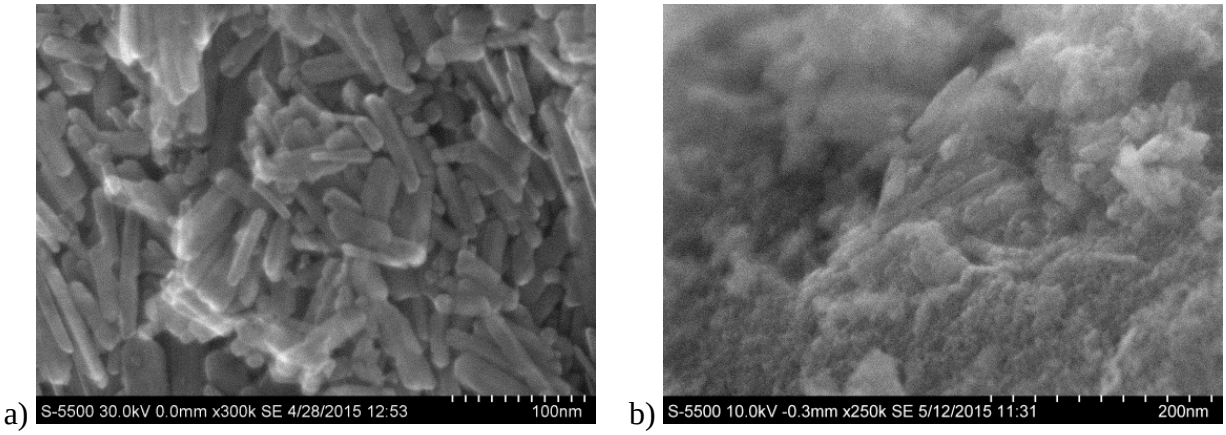

Figure 6 Scanning electron micrographs of a) Fe_2O_3 nanoparticles and b) the highly porous support matrix material (with Fe_2O_3 nanoparticles embedded).

7 CONCLUSIONS

We have presented a model for describing reaction-diffusion phenomena inside porous particles, including a novel grain-scale model. Our models account for transport limitations imposed by mass transfer to the surface of the porous support, pore diffusion, as well as diffusion and dissolution of reactive gases in the grains. The models are implemented in the open-source simulation tool *ParScale*, which is licensed under LGPL. This licensing model allows the linking of *ParScale* to any open-source and commercial particle-based flow solver.

We have demonstrated how an analytical solution of the governing equations, as well as numerical predictions of *ParScale* can be used to optimize the solids loading of the carrier particles. A key result is that the optimal loading level of active solid is close to the porosity of the support particle. Thus, the pores of the support particle should be filled by ca. 85% to 95% with the active solid, depending on the pore size of the support. In case the reactivity of the active solid is high (i.e., the reference Thiele modulus is large), only ca. 45% of the pore volume should be filled.

The current study was limited to a single heterogeneous reaction, and convective transport in the pores, as well as multi-component diffusion, was neglected. While the latter can be expected to have a negligible effect on our predictions, we expect that for reactions that result in a significant change in the gas-volume more work is needed. In these situations convective

transport in the pores might become important. Future work will show if this effect leads to a significant shift of the optimal solids loading.

AKNOWLEDGEMENT

The authors acknowledge support by the European Commission through FP7 Grant agreement no. 604656 ("NanoSim"). *LIGGGHTS*® is a registered trademark of DCS Computing GmbH.

REFERENCES

[1] Wei, G., He, F., Huang, Z., Zhao, K., Zheng, A., and Li, H., Chemical-Looping Reforming of Methane Using Iron Based Oxygen Carrier Modified with Low Content Nickel. *Chinese J. Chem.* (2014) **32**: 1271–1280.

[2] Adanez, J., Abad, A., Garcia-Labiano, F., Gayán, P., and de Diego, L.F., Progress in Chemical-Looping Combustion and Reforming technologies. *Prog. Energy Combust. Sci.* (2012) **38**: 215–282.

[3] Noorman, S., Gallucci, F., Van Sint Annaland, M., and Kuipers, J. a M., A theoretical investigation of CLC in packed beds. Part 1: Particle model. *Chem. Eng. J.* (2011) **167**: 297–307.

[4] Wen, C.Y., Noncatalytic solid fluid reactions. *Ind. Eng. Chem. Res.* (1968) **60**: 34–54.

[5] Han, L., Zhou, Z., and Bollas, G.M., Heterogeneous modeling of chemical-looping combustion. Part 1: Reactor model. *Chem. Eng. Sci.* (2013) **104**: 233–249.

[6] Han, L., Zhou, Z., and Bollas, G.M., Heterogeneous modeling of chemical-looping combustion. Part 2: Particle model. *Chem. Eng. Sci.* (2014) **113**: 116–128.

[7] Melchiori, T., and Canu, P., Improving the quantitative description of reacting porous solids: Critical analysis of the shrinking core model by comparison to the generalized grain model. *Ind. Eng. Chem. Res.* (2014) **53**: 8980–8995.

[8] Radl, S., Forgber, T., Kloss, C., and Aigner, A., ParScale - A Compilation of Particle Scale Models. (2015). Url: https://github.com/CFDEMproject/ParScale-PUBLIC.

[9] Agren, J., Oxidation and diffusion in oxides - a progress report, in: 10th NIST Diffus. Work., 2012. Url: http://www.nist.gov/mml/msed/thermodynamics_kinetics/upload/Agren-2012.pdf.

[10] Kattner, U.R., and Campbell, C.E., Modelling of thermodynamics and diffusion in multicomponent systems. *Mater. Sci. Technol.* (2009) **25**: 443–459.

[11] Monazam, E., and Breault, R., Thermogravimetric Analysis of Modified Hematite by Methane (CH4) for Chemical-Looping Combustion: A Global Kinetics Mechanism. *Ind. Eng. Chem. Res.* (2013) **52**: 14808–14816.

[12] Solunke, R.D., and Veser, G., Nanocomposite oxygen carriers for chemical-looping combustion of sulfur-contaminated synthesis gas. *Energy and Fuels*. (2009) **23**: 4787–4796.